

Scattering-matrix method for the tight-binding model of heterostructure electronic states

H. Taniyama and A. Yoshii

NTT LSI Laboratories, 3-1, Morinosato Wakamiya, Atsugi-shi, Kanagawa, 243-01, Japan

(Received 2 November 1995; revised manuscript received 27 December 1995)

Models of resonant-tunneling diodes based on the envelope-function approximation often give unsatisfactory results. In order to address some of the shortcomings of these models, we employ a tight-binding model that allows more careful treatment of heterointerfaces than is possible in the envelope-function approach. We use a scattering-matrix technique to carry out the calculation and present an improved method that allows us to calculate transfer across larger device dimensions. The method is applied to the calculation of transmission amplitudes for a single-barrier heterostructure.

I. INTRODUCTION

Semiconductor tunnel structures having negative differential resistance have been studied for many years. Interest in the development of resonant-tunneling structures grew due to rapid advances in semiconductor growth technology, such as molecular-beam epitaxy, that made it possible to control the composition and doping of the grown material on an atomic scale. This work has been followed by many other theoretical and experimental investigations into the tunneling process. For these structures, the simple one-band effective-mass model has been utilized to explain the main features of the tunneling. However, it is difficult to accommodate various critical factors such as the multiband and band-mixing effect, indirect-energy-band-gap and intervalley transfer, band non-parabolicity, and our understanding of the electronic structure of the semiconductor double-barrier quantum-well heterostructure remains incomplete.

Recently, it was reported that the X -point conduction-band minima play an important or dominant role in several heterostructures such as GaAs/AlAs.¹ Furthermore, the nearly lattice-matched InAs/GaSb/AlSb structure has received considerable attention because of the flexibility it offers for heterostructure design.^{2,3} Its interband tunneling nature comes from the fact that the tunneling involves the coupling between the InAs conduction- and the GaSb valence-band states. Devices built using this structure are attractive for use in high-frequency oscillators, logic circuits, and digital and analog applications. It has been recognized that the prediction and the analysis of electrical and optical properties of double-barrier quantum-well structures requires one to take into account the band structures of the constituent materials. The heterointerfaces must be treated more carefully than is possible in the usual envelope-function model. For the purpose of extending the model, one might try to extend the envelope-function approximation to include valley-mixing effects at a heterointerface.⁴⁻⁷ However, the connection rule of the envelope function at the heterointerface is very complicated and varying the location of the interface within a lattice constant leads to the deviation of the eigenenergies.⁸

Another method to treat semiconductor heterostructures is to use localized basis tight-binding models, which is the technique commonly used to calculate the bulk band struc-

ture. By employing the multiorbital tight-binding Hamiltonian, one can deal with the multiband effect, band-mixing effect, bulk-material-specific characteristics, and symmetry considerations in the constituent materials. Because all of these structures involve a lack of translational invariance on an atomic scale, a transfer-matrix approach is widely used. However, it is well known the transfer matrices used in these types of calculations are fraught with numerical instabilities, or in other words, exponential blowup. Schulman and co-workers,⁹⁻¹² Boykin, van der Wagt, and Harris,¹³ Ting, Yu, and McGill,¹⁴ and Stóvneng and Lipavský¹⁵ have addressed this problem by using some modified matrix methods. However, the transfer matrices in their models have a large dimension and the treated matrices are complicated. Ko and Inkson's model¹⁶ employed the scattering-matrix technique based on extended states at every transfer step, and in contrast to local-orbital-type models, it was based on a pseudopotential framework. Though their method is effective, it has never been extended to the tight-binding model.

In this work, we employ an sp^3s^* empirical tight-binding model to treat heterostructures lacking translational symmetry in one direction. To overcome the numerical instabilities and to make the formulation intuitively clear, we use a scattering-matrix approach for the electronic structures of semiconductor heterostructures, where the basis function is chosen as eigenvectors of a transfer matrix. The memory required is very small, i.e., proportional to the number of orbitals per unit cell. The method has been successfully applied to the calculation of transmission probabilities for GaAs/AlAs/GaAs and InAs/GaSb/InAs single-barrier structures and has been confirmed to be numerically stable in the calculation of the transmission coefficient for wide heterostructures.

In Sec. II, we define the current operator that exactly satisfies continuity. Using the eigenvectors of the transfer matrix and the current operator, we introduce the scattering matrix. In Sec. III, we demonstrate this numerical technique by calculating transmission probabilities of GaAs/AlAs/GaAs and InAs/GaSb/InAs single-barrier structures. Multiband effects on tunneling processes are explained there.

II. MODEL

A. Tight-binding model

We consider the heterostructure as a sequence of monolayers parallel to the heterointerfaces. Let M be the number

of orbitals per unit cell in our tight-binding basis set ($M = 10$ in our case). The basis orbitals may be written in the form $|\mathbf{R}_\parallel\sigma\alpha\rangle$, where σ is an integer monolayer label ($\sigma = 1, 2, \dots, N$), and $\alpha = 1, 2, \dots, M$ labels the orbitals within a unit cell. We consider the nearest-neighbor interaction in the calculation, in which each atomic plane is a layer. Since the in-plane crystal momentum, \mathbf{k}_\parallel , is a good quantum number, the wave function may be written as

$$|\psi\rangle = \sum_{\sigma,\alpha} C_{\sigma\alpha} |\sigma\alpha, \mathbf{k}_\parallel\rangle, \quad (1)$$

where $|\sigma\alpha, \mathbf{k}_\parallel\rangle$ is a planar orbital formed by taking Bloch sums of tight-binding orbitals over the N_\parallel unit cells in the σ th monolayer:

$$|\sigma\alpha, \mathbf{k}_\parallel\rangle = \frac{1}{\sqrt{N_\parallel}} \sum_{\mathbf{R}_\parallel} \exp(i\mathbf{k}_\parallel \cdot \mathbf{R}_\parallel) |\mathbf{R}_\parallel\sigma\alpha\rangle. \quad (2)$$

Here, \mathbf{R}_\parallel is the in-plane component of the unit cell coordinate.

In the tight-binding model, the Schrödinger equation is

$$H_{\sigma,\sigma-1} \mathbf{C}_{\sigma-1} + \bar{H}_{\sigma,\sigma} \mathbf{C}_\sigma + H_{\sigma,\sigma+1} \mathbf{C}_{\sigma+1} = 0, \quad (3)$$

where \mathbf{C}_σ is a vector of length M ,

$$\mathbf{C}_\sigma = \begin{pmatrix} C_{\sigma 1} \\ C_{\sigma 2} \\ \vdots \\ C_{\sigma M} \end{pmatrix}, \quad (4)$$

and $H_{\sigma,\sigma'}$ and $\bar{H}_{\sigma,\sigma}$ are $M \times M$ matrices whose elements are given by, respectively,

$$(H_{\sigma,\sigma'})_{\alpha,\alpha'} = \langle \sigma\alpha, \mathbf{k}_\parallel | H | \sigma'\alpha', \mathbf{k}_\parallel \rangle \quad (5)$$

and

$$(\bar{H}_{\sigma,\sigma'})_{\alpha,\alpha'} = \langle \sigma\alpha, \mathbf{k}_\parallel | (H - E) | \sigma'\alpha', \mathbf{k}_\parallel \rangle. \quad (6)$$

Equation (2) can be rewritten in an extended matrix formula as

$$\begin{pmatrix} \mathbf{C}_{\sigma-1} \\ \mathbf{C}_\sigma \end{pmatrix} = \begin{pmatrix} -H_{\sigma,\sigma-1}^{-1} \bar{H}_{\sigma,\sigma} & -H_{\sigma,\sigma-1}^{-1} H_{\sigma,\sigma+1} \\ 1 & 0 \end{pmatrix} \begin{pmatrix} \mathbf{C}_\sigma \\ \mathbf{C}_{\sigma+1} \end{pmatrix} \\ \equiv T_\sigma \begin{pmatrix} \mathbf{C}_\sigma \\ \mathbf{C}_{\sigma+1} \end{pmatrix}, \quad (7)$$

where T_σ is the so-called transfer matrix.

We may invoke the Bloch theorem to calculate the basis in the semi-infinite regions on either side of the device. In the nearest-neighbor interaction approximation, σ and $\sigma-2$ are layers composed of the same kinds of atoms, either anion or cation. Therefore, bulk states can be expressed as

$$B_\sigma = e^{ik_\perp d} B_{\sigma-2}. \quad (8)$$

Substituting Eq. (8) into Eq. (7), the bulk Bloch state is expressed as the eigenstate of the matrix equation,

$$T_{\sigma-1} T_\sigma \begin{pmatrix} B_\sigma \\ B_\sigma \end{pmatrix} = \lambda \begin{pmatrix} B_\sigma \\ B_\sigma \end{pmatrix}, \quad (9)$$

where $\lambda = e^{ik_\perp d}$ and k_\perp is the wave number. In the case of λ smaller than 1, the vector expresses the evanescent state, which cannot travel a long distance in the material.

B. Current continuity

In the envelope-function method, the transmission and reflection probability are calculated as the ratio of the current flow, which is carried by the incoming and outgoing states in the semi-infinite boundary of both sides. This definition of probabilities is legitimated by the continuity of the current whole through the system. However, it is not clear whether this definition of the current can be applied in this model. In the tight-binding model, probabilities are usually calculated as the ratio of the group velocities, $(1/\hbar) \partial E(k) / \partial k$, of incoming and outgoing states of both sides without the exact verification of the continuity of this current. In this section, we will define the exact conserving current carried by the basis state for the tight-binding model.

Let us introduce the value W , defined as

$$W_{\alpha\beta}(i) = C_\alpha^*(i) H_{i,i+1} C_\beta(i+1) - C_\alpha^*(i+1) H_{i+1,i} C_\beta(i), \quad (10)$$

where $C_{\alpha,\beta}(i)$ is the solution of the Schrödinger equation (2). This value $W(i)$ has layer dependency and can be interpreted as the matrix element of the operator,

$$\hat{W} \equiv \begin{pmatrix} 0 & H_{i,i+1}(\sigma) \\ H_{i+1,i}(\sigma) & 0 \end{pmatrix}. \quad (11)$$

The value $W(\sigma)$ can be probed so as to be conserved through all the layers. From the subtraction of Eq. (10) for neighboring layers, we obtain

$$\begin{aligned} W_{\alpha\beta}(i+1) - W_{\alpha\beta}(i) &= C_\alpha^*(i+1) H_{i+1,i+2} C_\beta(i+2) - C_\alpha^*(i+2) H_{i+2,i+1} C_\beta(i+1) - C_\alpha^*(i) H_{i,i+1} C_\beta(i+1) \\ &\quad + C_\alpha^*(i+1) H_{i+1,i} C_\beta(i) \\ &= C_\alpha^*(i+1) [H_{i+1,i+2} C_\beta(i+2) + H_{i+1,i} C_\beta(i)] - [C_\alpha^*(i+2) H_{i+2,i+1} + C_\alpha^*(i) H_{i,i+1}] C_\beta(i+1). \end{aligned} \quad (12)$$

By substituting the Schrödinger equation,

$$EC(i) = H_{i,i-1} C(i-1) + H_{i,i} C(i) + H_{i,i+1} C(i+1) \quad (13)$$

and its complex conjugate equation,

$$EC^*(i) = C^*(i-1)H_{i-1,i} + C^*(i)H_{i,i} + C^*(i+1)H_{i+1,i}, \quad (14)$$

into Eq. (12), we get

$$\begin{aligned} W_{\alpha\beta}(i+1) - W_{\alpha\beta}(i) &= C_{\alpha}^*(i+1)(E_{\beta} - H_{i+1,i+1})C_{\beta}(i+1) - C_{\alpha}^*(i+1)(E_{\alpha} - H_{i+1,i+1})C_{\beta}(i+1) \\ &= (E_{\beta} - E_{\alpha})C_{\alpha}^*(i+1)C_{\beta}(i+1). \end{aligned} \quad (15)$$

This equation represents the continuity of

$$W_{\alpha\beta}(i+1) - W_{\alpha\beta}(i) = 0 \quad (16)$$

for the solution of the Schrödinger equation with the same energy $E_{\alpha} = E_{\beta}$.

For the Bloch state, the coefficients $C_{\alpha,\beta}$ at each layer obey the relations

$$\begin{aligned} C_{\alpha}(i) &= \lambda_{\alpha}C_{\alpha}(i+2), \\ C_{\alpha}(i+1) &= \lambda_{\alpha}C_{\alpha}(i+3), \\ C_{\beta}(i) &= \lambda_{\beta}C_{\beta}(i+2), \\ C_{\beta}(i+1) &= \lambda_{\beta}C_{\beta}(i+3). \end{aligned} \quad (17)$$

Substituting Eq. (17) into

$$W_{\alpha\beta}(i) = C_{\alpha}^*(i)H_{i,i+1}C_{\beta}(i+1) - C_{\alpha}^*(i+1)H_{i+1,i}C_{\beta}(i) \quad (18)$$

yields

$$W_{\alpha\beta}(i) = \lambda_{\alpha}^*C_{\alpha}^*(i+2)H_{i+2,i+3}\lambda_{\beta}C_{\beta}(i+3) - \lambda_{\alpha}^*C_{\alpha}^*(i+3)H_{i+3,i+2}\lambda_{\beta}C_{\beta}(i+2) = \lambda_{\alpha}^*\lambda_{\beta}W_{\alpha\beta}(i+2). \quad (19)$$

For the states C_{α} and C_{β} which are the eigenvectors of Eq. (9) with eigenvalues λ_{α} and λ_{β} , the value of W also satisfies the following relation:

$$W_{\alpha\beta}(i+2) = W_{\alpha\beta}(i). \quad (20)$$

When C_{α} and C_{β} are the same traveling states, Eq. (19) represents current conservation and when C_{α} and C_{β} correspond to different traveling states, this equation means $W_{\alpha\beta} = 0$.

When state C is expressed as the linear combination of C_{α} and C_{β} ,

$$C = a_{\alpha}C_{\alpha} + a_{\beta}C_{\beta}. \quad (21)$$

The expectation value of \hat{W} for the state C is

$$\langle C | \hat{W} | C \rangle = |a_{\alpha}|^2 W_{\alpha\alpha} + |a_{\beta}|^2 W_{\beta\beta}. \quad (22)$$

This relation means that the components of the expectation value for the incoming state and reflected state can be separated and the total expectation value is the sum of each current component.

Because the value of W is imaginary, the electric current is defined with W as

$$J = e\hbar \text{Im}(W), \quad (23)$$

where Im means imaginary part.

J can be rewritten with the coefficient C explicitly as

$$J(i) = \text{Re} \left(\frac{e\hbar}{2i} C^*(i)H_{i,i+1}C(i+1) \right). \quad (24)$$

If we define the layer-dependent derivative in tight-binding form as

$$\nabla_i C(i) = H_{i,i+1}C(i+1) - H_{i,i}C(i), \quad (25)$$

$J(i)$ can be expressed as

$$J(i) = \text{Re} \left(\frac{e\hbar}{2i} C^*(i) \nabla_i C(i) \right), \quad (26)$$

which is a tight-binding form of the current and coincides with the usual definition of the current,

$$J = \text{Re} \left(\frac{e\hbar}{2i} \Psi^*(x) \nabla \Psi(x) \right), \quad (27)$$

in the envelope-function method.

C. Scattering matrix

The coefficients \mathbf{C} of the solution at the layers have the relation

$$\begin{pmatrix} \mathbf{C}_{\sigma-1} \\ \mathbf{C}_{\sigma} \end{pmatrix} = T_{\sigma} T_{\sigma+1} \begin{pmatrix} \mathbf{C}_{\sigma+1} \\ \mathbf{C}_{\sigma+2} \end{pmatrix}. \quad (28)$$

This equation relates the traveling states and evanescent states of a certain layer to the states of an adjacent layer in a certain direction of heterostructure. Treated states inevitably include exponentially divergent states as well as diminishing states. In matrix multiplication in the transfer-matrix method, this means that the multiplication of exponentially large numbers with exponentially small numbers is inevitable. Numerical errors will be introduced in this process.

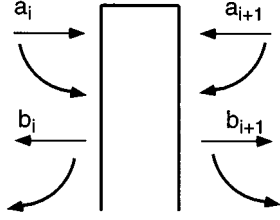


FIG. 1. The coefficients of eigenvectors of either side of an interface. Coefficient a_i corresponds to incoming states and b_i to outgoing states for a scattering matrix.

On the other hand, the scattering matrix relates incoming states with outgoing states. In general, which state is defined as the incoming state or outgoing state is arbitrary. If this definition is chosen properly, the calculation will include only small numbers. We define the direction of the propagation of states by the current for the traveling states or the direction of the evanescent state (see Fig. 1). In this method, there are only multiplications of small numbers, which reduces numerical error a great deal.

By eigenvectors of $T_\sigma T_{\sigma+1}$, state vectors are expressed as

$$\begin{pmatrix} \mathbf{C}_{\sigma-1} \\ \mathbf{C}_\sigma \end{pmatrix} = \mathbf{D}_\sigma \begin{pmatrix} \mathbf{a}_{\sigma-1} \\ \mathbf{b}_{\sigma-1} \end{pmatrix}, \quad (29a)$$

$$\begin{pmatrix} \mathbf{C}_{\sigma+1} \\ \mathbf{C}_{\sigma+2} \end{pmatrix} = \mathbf{D}_{\sigma+2} \begin{pmatrix} \mathbf{a}_{\sigma+1} \\ \mathbf{b}_{\sigma+1} \end{pmatrix}. \quad (29b)$$

\mathbf{D}_σ is a $2M \times 2M$ matrix whose column vectors are the eigenvectors of $T_\sigma T_{\sigma+1}$ and, for convenience, the eigenvectors are sorted according to their direction of propagation. Using the same basis, the transfer matrix is

$$\mathbf{D}_\sigma^{-1} T_\sigma T_{\sigma+1} \mathbf{D}_{\sigma+2} = M_\sigma. \quad (30)$$

With this representation, Eq. (28) is rewritten as

$$\begin{pmatrix} \mathbf{a}_{\sigma-1} \\ \mathbf{b}_{\sigma-1} \end{pmatrix} = M_\sigma \begin{pmatrix} \mathbf{a}_{\sigma+1} \\ \mathbf{b}_{\sigma+1} \end{pmatrix}. \quad (31)$$

Changing the order of elements to all incoming states to the right-hand side and outgoing states to the left, this equation is written in the scattering matrix form,

$$\begin{pmatrix} \mathbf{b}_{\sigma-1} \\ \mathbf{b}_{\sigma+1} \end{pmatrix} = \begin{pmatrix} M_{21} M_{11}^{-1} & M_{22} - M_{21} M_{11}^{-1} M_{12} \\ M_{11}^{-1} & -M_{12} \end{pmatrix} \begin{pmatrix} \mathbf{a}_{\sigma-1} \\ \mathbf{a}_{\sigma+1} \end{pmatrix}. \quad (32)$$

This equation relates the coefficient of the incoming state from either layer to the outgoing state. When we have two S matrices of adjacent layers,

$$\begin{pmatrix} \mathbf{b}_{\sigma-1} \\ \mathbf{b}_{\sigma+1} \end{pmatrix} = \begin{pmatrix} S_{11}^A & S_{12}^A \\ S_{21}^A & S_{22}^A \end{pmatrix} \begin{pmatrix} \mathbf{a}_{\sigma-1} \\ \mathbf{a}_{\sigma+1} \end{pmatrix}, \quad (33a)$$

and

$$\begin{pmatrix} \mathbf{b}_{\sigma+1} \\ \mathbf{b}_{\sigma+3} \end{pmatrix} = \begin{pmatrix} S_{11}^B & S_{12}^B \\ S_{21}^B & S_{22}^B \end{pmatrix} \begin{pmatrix} \mathbf{a}_{\sigma+1} \\ \mathbf{a}_{\sigma+3} \end{pmatrix}, \quad (33b)$$

the combined S matrix for these layers is

$$\begin{pmatrix} \mathbf{b}_{\sigma-1} \\ \mathbf{b}_{\sigma+3} \end{pmatrix} = \begin{pmatrix} S_{11} & S_{12} \\ S_{21} & S_{22} \end{pmatrix} \begin{pmatrix} \mathbf{a}_{\sigma-1} \\ \mathbf{a}_{\sigma+3} \end{pmatrix}, \quad (34)$$

where matrices S_{ij} are

$$S_{11} = S_{11}^\sigma + S_{12}^\sigma (1 - S_{11}^{\sigma+2} S_{22}^\sigma)^{-1} S_{11}^{\sigma+2} S_{21}^\sigma, \quad (35a)$$

$$S_{12} = S_{12}^\sigma (1 - S_{11}^{\sigma+2} S_{22}^\sigma)^{-1} S_{12}^{\sigma+2}, \quad (35b)$$

$$S_{21} = S_{21}^\sigma (1 - S_{22}^\sigma S_{11}^{\sigma+2})^{-1} S_{21}^\sigma, \quad (35c)$$

$$S_{22} = S_{22}^{\sigma+2} + S_{21}^\sigma (1 - S_{22}^\sigma S_{11}^{\sigma+2})^{-1} S_{22}^\sigma S_{12}^{\sigma+2}. \quad (35d)$$

By performing these procedures successively, we can obtain the final S matrix that expresses the transition of states between the semi-infinite regions on either side of the device.

To calculate the scattering state for the heterostructure, the boundary condition for these semi-infinite regions is set as

$$|\psi; L\rangle = I_0 |J_0^+; L\rangle + \sum_{j=1}^M r_j |J_{j+M}^-; L\rangle, \quad (36a)$$

$$|\psi; R\rangle = \sum_{j=1}^M t_j |J_j^+; R\rangle, \quad (36b)$$

where $|\psi; L\rangle$ and $|\psi; R\rangle$ are the states in the left and right regions and J^+ and J^- express the positive and negative current states, i.e., propagating to the right and left, respectively. With the S matrix, the relation between coefficients t_j and r_i is

$$\begin{pmatrix} \mathbf{r} \\ \mathbf{t} \end{pmatrix} = \begin{pmatrix} \mathbf{S}_{11} & \mathbf{S}_{12} \\ \mathbf{S}_{21} & \mathbf{S}_{22} \end{pmatrix} \begin{pmatrix} \mathbf{I}_0 \\ \mathbf{0} \end{pmatrix}. \quad (37)$$

The transmission and reflection probabilities can be defined as the ratio between the current flow in the semi-infinite region of either side of the heterostructure. The transmission probability is

$$T = \sum_i |t_i|^2 \frac{J_i^+}{J_0^+}, \quad (38)$$

where J_i^+ is the current calculated by $\langle J_i^+; R | J | J_i^+; R \rangle$ and J_0^+ is $\langle J_0^+; L | J | J_0^+; L \rangle$. The summation is performed for all right-traveling states in the right semi-infinite region. The reflection probability is

$$R = \sum_i |r_i|^2 \frac{J_{i+M}^-}{J_0^+}, \quad (39)$$

where the summation is performed for all left-traveling states in the left semi-infinite region.

III. RESULTS

In this section we present the results of a systematic study of electron tunneling in single-barrier structures to illustrate the stability of the technique. No problems were encountered with the scattering-matrix method even for systems as large as 1500 Å. The transfer-matrix method, however, failed for systems as large as 150 Å. Furthermore, the method has a

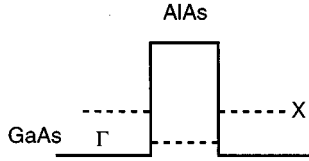


FIG. 2. Energy-band diagram of an GaAs/AlAs/GaAs single-barrier structure. The solid lines depict the band edges at the Γ point and the dashed lines depict the X point of AlAs.

memory cost proportional to the number of considered orbitals in a layer and not to the number of layers. We use the same tight-binding parameters used by Boykin, van der Wagt, and Harris¹³ for GaAs and AlAs, which include the amount of band discontinuity between GaAs and AlAs. For InAs and GaSb, we use the parameters used by Vogl, Hjalmarson, and Dow.¹⁷

A. GaAs/AlAs/GaAs single-barrier structure

We shall first investigate the heterostructure composed of GaAs and AlAs, which is an indirect-gap semiconductor. Figure 2 shows a schematic energy-band diagram for the GaAs/AlAs/GaAs single-barrier structure. In ordinary approaches using the envelope function, the effective mass at the Γ state band edge for each material is used, and the X point or L point of AlAs is not considered. However, it has been indicated that X -point conduction-band minima play an important role.¹

The bulk-band structure is calculated from the eigenvalues of the transfer matrix as in Eq. (8). Figure 3 shows the band structures for the GaAs and AlAs in the $[111]$ and $[100]$ directions. In the $[111]$ direction, the L state of AlAs is lower than the Γ state and near to the L state of GaAs. In the $[100]$ direction, the AlAs X -valley minimum is very low compared to the Γ state and comparable to the GaAs Γ -state energy. The second GaAs X_2 state and AlAs X_2 are also lower than the AlAs Γ state, so traversing through these states becomes important in the GaAs/InAs heterostructure.

Figure 4 shows the effects of varying barrier widths on the transmission amplitude. For energies smaller than the AlAs L -valley minimum, the diminishing amplitude of the wave function in the AlAs layer decreases the transmission probabilities for the large barrier width, as expected. However, the transmission probabilities oscillate for energies higher than the AlAs L -valley minimum. The period of this oscillation becomes small for large barrier widths. For energies larger than the AlAs L -valley minimum, the probability has a value around 0.01 for wide AlAs layers. Antiresonance appears around 0.5 eV, which corresponds to the GaAs L -valley minimum. The details of these characteristics can be clarified by the transmission probability to the GaAs L valley.

Figure 5 shows the probability of transmission from the GaAs Γ state to the GaAs L state. For narrow AlAs layers, the transmission probability is large throughout the calculated energy region. For wide AlAs layers, the probability for the energy range from the GaAs L -valley minimum to the AlAs L -valley minimum becomes small. This is because for these energies there are no traveling states in AlAs and the

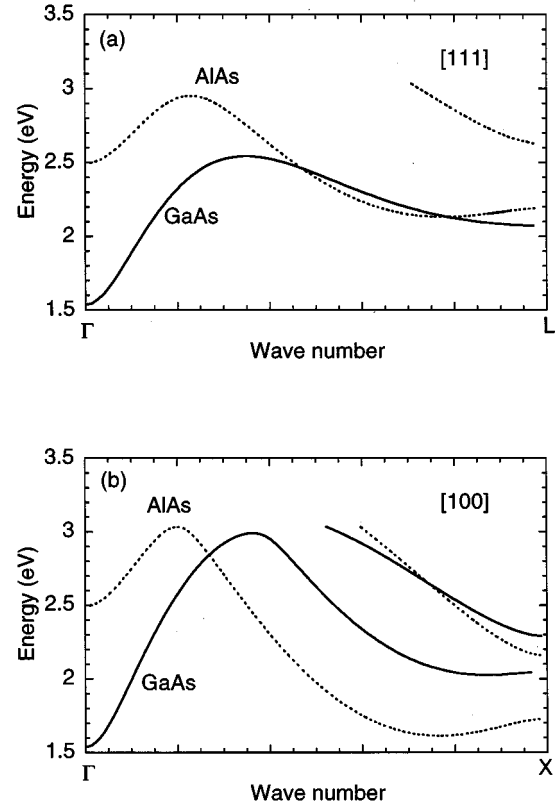


FIG. 3. Band structure of GaAs and AlAs (a) in the $[111]$ direction and (b) in the $[100]$ direction.

amplitude is evanescent. For energies larger than the AlAs L -valley minimum, an electron inserted into the GaAs Γ state traverses to the AlAs L -valley state, which is not an evanescent state. The figure shows a probability value of around 0.1 for large barrier width. This suggests that the transmission from the resonance is due to the resonant tunneling through the quasibound states. The antiresonance is due to destructive interference between the Γ - X - Γ and the Γ - Γ - Γ channels.

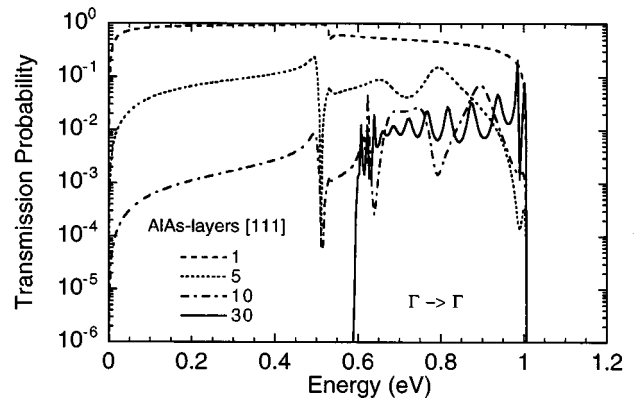


FIG. 4. Transmission probability for the GaAs/AlAs/GaAs single-barrier structure in the $[111]$ direction as a function of electron energy for four structures with different barrier widths. The electron is incident from the Γ valley of the GaAs with $\mathbf{k}_{\parallel}=0$ and transfers to the Γ valley of the GaAs. Energy is referenced from the GaAs Γ -valley minimum in the figure.

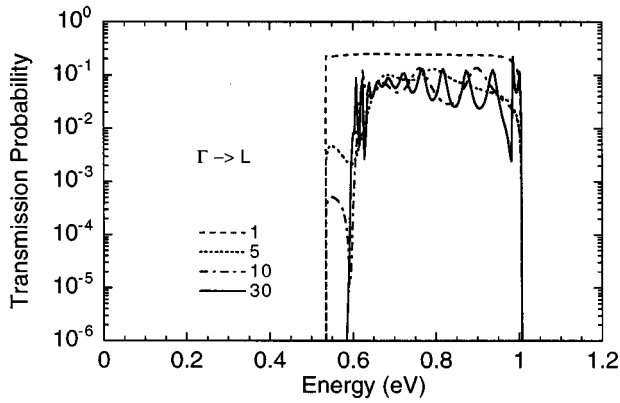


FIG. 5. Transmission probability for the GaAs/AlAs/GaAs single-barrier structure in the [111] direction as a function of electron energy for four structures with different barrier widths. The electron is incident from the Γ valley of the GaAs with $\mathbf{k}_{\parallel}=0$ and transfers to the L valley of the GaAs. Energy is referenced from the GaAs Γ -valley minimum in the figure.

For the [100] direction, the transmission probability shows complex characteristics because of the low AlAs X -valley minimum and because of the contributions of the second X_2 valley of GaAs and AlAs. Figure 6 shows the effects of varying the barrier width on the transmission amplitude for the state inserting into the Γ state of GaAs transmitting in the Γ state of GaAs. For the energy range from the GaAs conduction-band minimum to the AlAs X -valley minimum, the transmission probability decreases for large AlAs layer widths. For energies between the AlAs X -valley minimum and the GaAs X -valley minimum, probability resonance appears and its energy half-width and its interval become narrow. In this process, the Γ - X - Γ channel is the main contributor. From the GaAs X -valley minimum to AlAs Γ -valley minimum, Γ - X transfer and Γ - X_2 transfer occur as well as Γ - Γ and for energies larger than the AlAs Γ -valley minimum, the Γ - Γ probability represents resonance characteristics similar to the results obtained by the envelope-

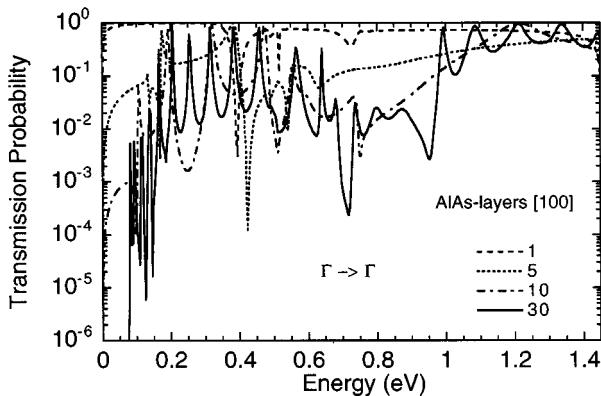


FIG. 6. Transmission probability for the GaAs/AlAs/GaAs single-barrier structure in the [100] direction as a function of electron energy for four structures with different barrier widths. The electron is incident from the Γ valley of the GaAs with $\mathbf{k}_{\parallel}=0$ and transfers to the Γ valley of the GaAs. Energy is referenced from the GaAs Γ -valley minimum in the figure.

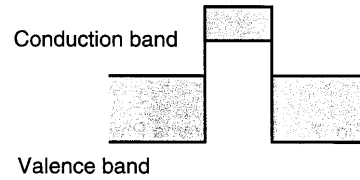


FIG. 7. Energy-band diagram of an InAs/GaSb/InAs single-barrier structure. The lines depict the band edges at the Γ point.

function method. The resonances are related to quasibound states localized in the AlAs layers by the effective quantum-well potential defined by the X and X_2 minima profiles.

B. InAs/GaSb/InAs single-barrier structure

Figure 7 shows a schematic energy-band diagram for the InAs/GaSb/InAs single-barrier structure. At the flat bias condition, electrons inserted into the InAs conduction band will traverse to the GaSb valence band and finally to the InAs conduction band. Under certain bias conditions, electrons inserted into the InAs conduction band will be blocked by the band gap of GaSb. This structure has attracted much interest for device applications. Figure 8 shows the band structure for InAs and GaSb bulk in the [111] direction. The valence-band edge of GaSb is higher than the conduction-band edge of InAs for 0.15 eV and the band gap of GaSb is about 0.78 eV. Incoming electrons with energies below 0.15 eV in the InAs conduction band will traverse through the valence-band state, without dropping in amplitudes. However, incoming electrons with energies corresponding to the GaSb band gap will be blocked.

The transmission probability from the InAs Γ state to InAs Γ state in the [111] direction is shown in Fig. 9 as a function of GaSb layer width. The transmission probability is smaller for larger GaSb layer widths: In particular, the probability for energies from 0.15 eV to 0.93 eV is greatly suppressed with the width of the GaSb layer because this region corresponds to the band gap of GaSb. For a comparatively narrow GaSb layer, however, the blocking effect of the band gap is not conspicuous. For wider GaSb layers, the transmission probability for these energies becomes small and the blocking effects of the band gap become apparent. For energies smaller than 0.15 eV, where electrons traverse through the GaSb valence band, resonance characteristics appear for wide GaSb. The resonance is related to quasibound states

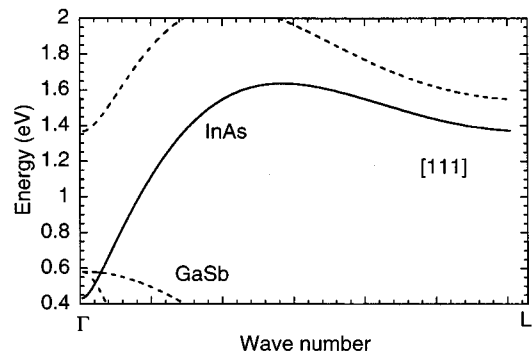


FIG. 8. Band structure of InAs and GaSb in the [111] direction.

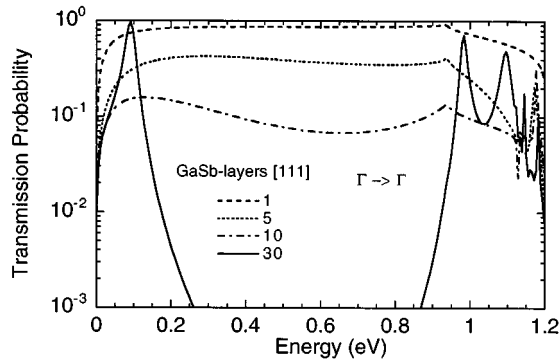


FIG. 9. Transmission probability for the InAs/GaSb/InAs single-barrier structure in the [111] direction as a function of electron energy for four structures with different barrier widths. The electron is incident from the Γ valley of the InAs with $k_{\parallel}=0$ and transfers to the Γ valley of the InAs. Energy is referenced from the GaAs Γ -valley minimum in the figure.

localized in the GaSb layers by the effective quantum-well potential defined by the valence-band-edge profile. For energies higher than 0.93 eV, similar resonance appears. These resonances are attributed to quasibound states localized in the GaSb layers by the effective quantum-well potential defined by the L minima profile. Above the second GaSb L -valley minimum, the transmission probability becomes complicated because of the contribution of the channel through the L -valley state. However, the transmission probability in the [100] direction does not show this complicated resonance structure within the calculated energy, because in the [100] direction the X_2 -valley minimum energy is much larger.

Figure 10 shows the transmission probabilities for a wide GaSb layer (300 ML). In this structure, the blocking effect of the GaSb band gap is clear and many resonances appear in the Γ - H - Γ transmission below 0.15 eV and in the transmis-

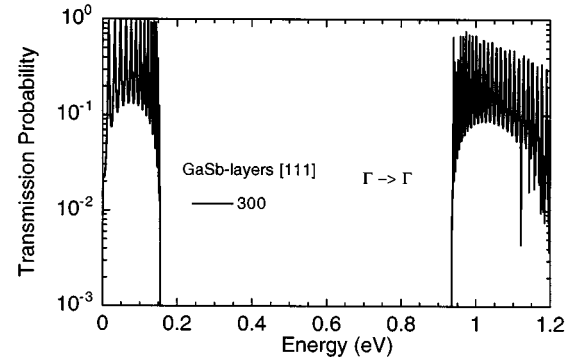


FIG. 10. Transmission probability for the InAs/GaSb/InAs single-barrier structure in the [100] direction as a function of electron energy for 300 layers of GaSb. The electron is incident from the Γ valley of the InAs with $k_{\parallel}=0$ and transfers to the L valley of the InAs. Energy is referenced from the GaAs Γ -valley minimum in the figure.

sion probability beyond 0.93 eV. The half-width of the resonant peaks and the distances between peaks are very small because of the wide effective quantum-well width in GaSb.

IV. CONCLUSIONS

We have formulated a tight-binding model by introducing an S -matrix description based on a detailed discussion of the definition of conserving current. Our method is numerically stable, efficient, and simple to implement, making it possible to compute transmission coefficients effectively in wide heterostructures using realistic multiband band-structure models.

ACKNOWLEDGMENTS

The authors would like to thank Dr. M. Tomizawa, Dr. T. Waho, H. Kitabayashi, and Dr. M. Yamamoto for helpful discussions. The authors also wish to thank Dr. Y. Imamura for his encouragement.

¹M. K. Jackson, D. Z. -Y. Ting, D. H. Chow, and D. A. Collins, Phys. Rev. B **43**, 4856 (1991).

²J. N. Schulman, D. H. Chow, and T. C. Hasenberger, Solid State Electron. **37**, 981 (1994).

³Y. H. Wang, M. H. Liu, M. P. Houg, J. F. Chen, and A. Y. Cho, IEEE. Trans. Electron. Devices **41**, 1734 (1994).

⁴T. Ando, S. Wakahara, and H. Aker, Phys. Rev. B **40**, 11 609 (1989).

⁵T. Ando and H. Aker, Phys. Rev. B **40**, 11 619 (1989).

⁶T. Ando, Phys. Rev. B **47**, 9621 (1993).

⁷G. T. Einevoll and L. J. Sham, Phys. Rev. B **49**, 10 533 (1994).

⁸T. L. Li and K. J. Kuhn, Phys. Rev. B **49**, 2608 (1994).

⁹J. N. Schulman and Y.-C. Chang, Phys. Rev. B **27**, 2346 (1983).

¹⁰J. N. Schulman and Y.-C. Chang, Phys. Rev. B **31**, 2056 (1985).

¹¹J. N. Schulman and M. Waldner, J. Appl. Phys. **63**, 2859 (1988).

¹²J. N. Schulman and D. Z. Y. Ting, Phys. Rev. B **45**, 6282 (1992).

¹³T. B. Boykin, J. P. A. van der Wagt, and J. J. S. Harris, Phys. Rev. B **43**, 4777 (1991).

¹⁴D. Z. Y. Ting, E. T. Yu, and T. C. McGill, Phys. Rev. B **45**, 3583 (1992).

¹⁵J. A. Støvneng and P. Lipavsky, Phys. Rev. B **49**, 16 494 (1994).

¹⁶Y. K. Ko and J. C. Inkson, Phys. Rev. B **38**, 9945 (1988).

¹⁷P. Vogl, H. P. Hjalmanson, and J. D. Dow, J. Phys. Chem. Solids **44**, 365 (1983).